NuSTAR View of the Black Hole Wind in the Galaxy Merger IRAS F11119+3257

F. Tombesi[1,2,3] , S. Veilleux[2,4] , M. Meléndez[2,3,5] , A. Lohfink[6,7], J. N. Reeves[8], E. Piconcelli[9], F. Fiore[9], and C. Feruglio[10,11]

[1] Department of Physics, University of Rome "Tor Vergata," Via della Ricerca Scientifica 1, I-00133 Rome, Italy; francesco.tombesi@roma2.infn.it
[2] Department of Astronomy, University of Maryland, College Park, MD 20742, USA; ftombesi@astro.umd.edu
[3] NASA/Goddard Space Flight Center, Code 662, Greenbelt, MD 20771, USA; francesco.tombesi@nasa.gov
[4] Joint Space-Science Institute, University of Maryland, College Park, MD 20742, USA
[5] Wyle Science, Technology and Engineering Group, 1290 Hercules Avenue, Houston, TX 77058 USA
[6] Institute of Astronomy, Madingley Road, Cambridge, CB3 0HA, UK
[7] Department of Physics, Montana State University, P.O. Box 173840, Bozeman, MT 59717-3840, USA
[8] Astrophysics Group, School of Physical and Geographical Sciences, Keele University, Keele, Staffordshire, ST5 5BG, UK
[9] INAF Osservatorio Astronomico di Roma, Via Frascati 33, I-00078 Monteporzio Catone, Italy
[10] INAF Osservatorio Astronomico di Trieste, Via G.B. Tiepolo 11, I-34143 Trieste, Italy
[11] Scuola Normale Superiore, Piazza dei Cavalieri 7, I-56126 Pisa, Italy

Abstract

Galactic winds driven by active galactic nuclei (AGNs) have been invoked to play a fundamental role in the co-evolution between supermassive black holes and their host galaxies. Finding observational evidence of such feedback mechanisms is of crucial importance and it requires a multi-wavelength approach in order to compare winds at different scales and phases. In Tombesi et al., we reported the detection of a powerful ultra-fast outflow (UFO) in the *Suzaku* X-ray spectrum of the ultra-luminous infrared galaxy IRAS F11119+3257. The comparison with a galaxy-scale OH molecular outflow observed with *Herschel* in the same source supported the energy-conserving scenario for AGN feedback. The main objective of this work is to perform an independent check of the *Suzaku* results using the higher sensitivity and wider X-ray continuum coverage of *NuSTAR*. We clearly detect a highly ionized Fe K UFO in the 100 ks *NuSTAR* spectrum with parameters $N_{\rm H} = (3.2 \pm 1.5) \times 10^{24}\,{\rm cm}^{-2}$, $\log \xi = 4.0^{+1.2}_{-0.3}\,{\rm erg\,s}^{-1}\,{\rm cm}$, and $v_{\rm out} = 0.253^{+0.061}_{-0.118}c$. The launching radius is likely at a distance of $r \geqslant 16 r_s$ from the black hole. The mass outflow rate is in the range of $\dot{M}_{\rm out} \simeq 0.5\text{–}2\,M_\odot\,{\rm yr}^{-1}$. The UFO momentum rate and power are $\dot{P}_{\rm out} \simeq 0.5\text{–}2\,L_{\rm AGN}/c$ and $\dot{E}_{\rm out} \simeq 7\%\text{–}27\%\,L_{\rm AGN}$, respectively. The UFO parameters are consistent between the 2013 *Suzaku* and the 2015 *NuSTAR* observations. Only the column density is found to be variable, possibly suggesting a clumpy wind. The comparison with the energetics of molecular outflows estimated in infrared and millimeter wavelengths support a connection between the nuclear and galaxy-scale winds in luminous AGNs.

Key words: black hole physics – galaxies: active – line: identification – X-rays: galaxies

1. Introduction

It has been suggested that mergers between gas-rich galaxies can possibly trigger major starbursts, enhance the growth of supermassive black holes (SMBHs), and, ultimately, lead to the formation of red gas-poor elliptical galaxies (e.g., Hopkins et al. 2006). In this galaxy merger scenario, as dust and gas is gradually dispersed, a completely obscured ultra-luminous infrared galaxy (ULIRG) evolves to a dusty quasar, and finally to a completely exposed quasar. Galactic winds driven by the central active galactic nucleus (AGN) and/or the surrounding starburst have been invoked to play a fundamental role in this phase, quenching the growth of both the SMBH and stellar spheroidal component, and possibly explaining the tight SMBH-spheroid mass relations (e.g., Silk & Rees 1998; King 2003; King & Pounds 2003; Gaspari & Sądowski 2017). Finding observational evidence of such feedback mechanism(s) is of crucial importance to understand galaxy and SMBH evolution (e.g., Fiore et al. 2017).

In order to inhibit star formation, outflows have to affect the molecular gas out of which stars form. Far-infrared molecular spectroscopy with Herschel of ULIRGs provided a break-through in identifying and analyzing these massive molecular outflows. In particular, OH absorption observations have revealed molecular outflows at hundreds of parsec scales with high velocities, up to maximum values of $1200\,{\rm km\,s}^{-1}$,

implying significant mass outflow rates up to $150\text{–}1500\,M_\odot\,{\rm yr}^{-1}$ (e.g., Sturm et al. 2011; Veilleux et al. 2013; González-Alfonso et al. 2014, 2017).

Several models have been suggested in order to explain their origin, but essentially all of them require an initial very fast ($v_{\rm out} \sim 0.1c$) AGN accretion disk wind driving a shock into the host galaxy interstellar medium, and the molecular material is removed by the resultant hot shocked bubble (e.g., Faucher-Giguère & Quataert 2012; Zubovas & King 2012; Costa et al. 2014). The shock caused by the interaction between the fast wind and the host galaxy interstellar medium divides the resultant large-scale outflow in two regimes. Momentum-conserving flows occur if most of the wind kinetic energy is radiated away. In this case, radiation and ram pressure exert work on the interstellar medium gas. Instead, energy-conserving flows occur if the shocked wind gas is not efficiently cooled, and instead expands adiabatically as a hot bubble. In particular, it is expected that the momentum flux of the outflow in the energy-conserving case would be larger than that of the radiation, up to values of $\dot{P} \simeq 10 L_{\rm AGN}/c$ as observed in several ULIRGs (e.g., Sturm et al. 2011; Cicone et al. 2014; González-Alfonso et al. 2017). However, despite these significant developments, observational evidences for the connection between the putative nuclear fast AGN wind and the large-scale outflows are difficult to find.

Blueshifted Fe XXV/XXVI absorption lines at $E > 7\,\mathrm{keV}$ have been detected in the X-ray spectra of several AGNs. Often, the implied velocity is very high, up to the mildly relativistic values of $v_{\mathrm{out}} \simeq 0.1\,c$ for the so-called ultra-fast outflows (UFOs; e.g., Tombesi et al. 2010, 2011, 2014, 2015; Gofford et al. 2013; Longinotti et al. 2015; Nardini et al. 2015; Parker et al. 2017). These winds are observable at sub-parsec scales from the central black hole, consistently with an accretion disk interpretation, and they seem to be powerful enough to have a substantial effect on the host galaxy environment (e.g., Tombesi et al. 2012, 2015, Wagner et al. 2013; Gofford et al. 2015; Nardini et al. 2015).

Recently, a 250 ks *Suzaku* observation of IRAS F11119 +3257 obtained by our group in 2013 showed the presence of a powerful UFO with a velocity of $v_{\mathrm{out}} \simeq 0.25c$ in this ultra-luminous infrared galaxy hosting a large-scale molecular outflow (Tombesi et al. 2015). Comparing the energetics of these two winds, we found support for the validity of the energy-conserving mechanism connecting the inner black hole winds to the large-scale molecular outflows (e.g., Faucher-Giguère & Quataert 2012; Zubovas & King 2012). An analogous conclusion was reached by Feruglio et al. (2015) for the ULIRG/quasar Mrk 231.

2. The Galaxy IRAS F11119+3257

IRAS F11119+3257 is a ULIRG at $z = 0.189$ with an AGN dominated quasar-like luminosity of $L_{\mathrm{AGN}} \simeq 1.5 \times 10^{46}\,\mathrm{erg\,s^{-1}}$ (Veilleux et al. 2013). This source was previously observed with *Chandra* for a 15 ks snapshot exposure as part of the quasar and ULIRG evolution study (QUEST) campaign (Teng & Veilleux 2010). It provides a very good combination of X-ray brightness and moderate neutral absorption in the QUEST survey, making it a promising candidate to study the Fe K band absorbers in this type of object.

The data to model ratios of our 250 ks *Suzaku* observation obtained in 2013 May with respect to an absorbed ($N_{\mathrm{H}} \simeq 2 \times 10^{22}\,\mathrm{cm^{-2}}$) power-law continuum ($\Gamma \simeq 2$) showed the presence of strong absorption residuals in the energy range $E \simeq 8$–$10\,\mathrm{keV}$ and a factor of ~ 3 hard excess at energies of $E \simeq 15$–$25\,\mathrm{keV}$ (Tombesi et al. 2015). The absorption is well modeled with a broad inverted Gaussian line with parameters $E = 9.82^{+0.64}_{-0.34}\,\mathrm{keV}$, $\sigma_E = 1.67^{+1.00}_{-0.44}\,\mathrm{keV}$, and equivalent width $\mathrm{EW} = -1.31^{+0.40}_{-0.31}\,\mathrm{keV}$ with a high detection confidence level of 6.5σ.

If identified with absorption from Fe XXV–XXVI, this feature would indicate a high blueshifted velocity of $v_{\mathrm{out}} \simeq 0.2$–$0.3\,c$. Indeed, a fit using a dedicated *XSTAR* table (Kallman & Bautista 2001) with a velocity broadening of $30{,}000\,\mathrm{km\,s^{-1}}$ provides the best representation of the data, compared to an absorption edge or relativistic reflection (Tombesi et al. 2015). The highly ionized absorber has a column density $N_{\mathrm{H}} = (6.4^{+0.8}_{-1.3}) \times 10^{24}\,\mathrm{cm^{-2}}$, an ionization parameter $\log\xi = 4.11^{+0.09}_{-0.04}\,\mathrm{erg\,s^{-1}\,cm}$, and an outflow velocity of $v_{\mathrm{out}} = 0.255 \pm 0.011c$.

This fast wind model allows us to simultaneously fit both the Fe K absorption and the hard excess. However, we note that these two spectral features, fundamental for the interpretation as a fast wind, may have some ambiguities in the *Suzaku* data given that they are detected in two separate instruments. In particular, the broad absorption is at the high-energy end of the XIS bandpass and the high-energy detector PIN is a nonimaging background dominated instrument. Moreover, the XIS and PIN do not overlap in energy, which is important for
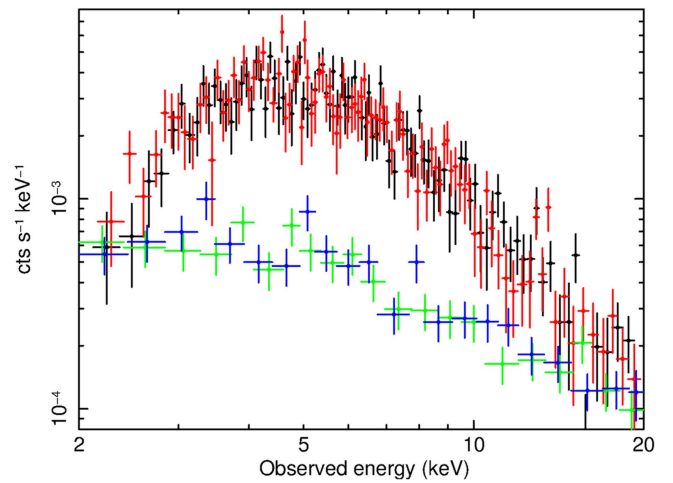
Figure 1. Separated *NuSTAR* FPMA/FPMB source (black/red) and background (green/blue) spectra of IRAS F11119+3257. The data are rebinned to a minimum of 25 counts per bin and no cross-normalization correction is applied.

placing the right continuum level at the energies between $E \simeq 10\,\mathrm{keV}$. An analysis of the *NuSTAR* spectrum would allow us to have an important independent check on the presence of the UFO in this ULIRG and to simultaneosly constrain the hard X-ray continuum up to energies of $E \simeq 30\,\mathrm{keV}$.

3. NuSTAR Data Analysis and Results

Here, we describe the spectral analysis of the *NuSTAR* observation of IRAS F11119+3257 performed in May 2015 (obsID 60101045002). The *NuSTAR* data were reduced following the standard procedure, using the *nupipeline* and *nuproducts* scripts available in the NuSTARDAS software package. We used NuSTARDAS version 1.4.1 and the calibration version. We extracted the source spectrum from a circular region with a 70 arcsec radius, centered on the peak of the point-source image. The background spectra for each focal plane module (FPM), FPMA and FPMB, were extracted from a polygonal region on the detector containing the source and avoiding the area 90 arcsec around the peak. We use the data taken in standard SCIENCE mode, with a total exposure of 104 ks.

The spectral analysis was performed in the energy interval $E = 2$–$20\,\mathrm{keV}$ using the software *XSPEC* v.12.8.2. We grouped the data to a minimum of 25 counts per bin in order to apply the χ^2-statistic. We performed joint fits for the two separated FPMA and FPMB detectors and the spectra were merged only for plotting purposes. In all the models, we include a cross-normalization parameter for the two detectors, which was found to be within 8%. All parameters are given in the source rest frame and the errors are at the 1σ level if not otherwise stated. Standard solar abundances are assumed (Asplund et al. 2009).

In Figure 1, we show the source spectra of the two detectors and the relative backgrounds. We note that the source is clearly detected over the background in the whole $E = 2$–$20\,\mathrm{keV}$ observed energy band and the spectra taken by the two detectors agree very well in both slope and normalization. The observed flux is the $E = 2$–$10\,\mathrm{keV}$ and $E = 10$–$20\,\mathrm{keV}$ energy bands is $1 \times 10^{-12}\,\mathrm{erg\,s^{-1}\,cm^{-2}}$ and $4 \times 10^{-13}\,\mathrm{erg\,s^{-1}\,cm^{-2}}$, respectively.
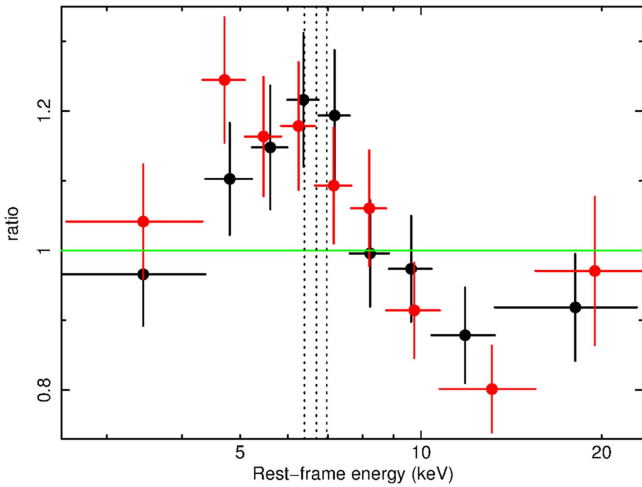
Figure 2. Ratio between the *NuSTAR* spectrum and an absorbed $\Gamma = 2$ power-law continuum model. The *NuSTAR* FPMA and FPMB data are shown in black and red, respectively. The vertical dotted lines indicate the rest-frame energies for Fe Kα at $E = 6.4$ keV, Fe XXV Heα at $E = 6.7$ keV, and the Fe XXVI Lyα at $E = 6.97$ keV, respectively. The data are binned to a minimum signal-to-noise of 13 for clarity. The P-Cygni emission/absorption profile is evident in the data.

3.1. Spectral Analysis

A neutral Galactic absorption of $N_H = 2.1 \times 10^{21}$ cm^{-2} modeled with *wabs* in *XSPEC* is included in all the fits (Kalberla et al. 2005). We started the spectral modeling with an absorbed continuum power law with $\Gamma \simeq 2$ ($\chi^2/\nu = 210/183$). The inclusion of an intrinsic neutral absorption component *zwabs* of $N_H = 2.1 \times 10^{22}$ cm^{-2} as found in *Suzaku* is not statistically required here because *NuSTAR* is not sensitive at energies below $E = 2$ keV.

In Figure 2, we show the ratio of the *NuSTAR* data with respect to the absorbed $\Gamma = 2$ power-law continuum. We can observe broad emission residuals redward of the main Fe K emission lines (vertical lines indicating Fe Kα at $E = 6.4$ keV, Fe XXV Heα at $E = 6.7$ keV, and the Fe XXVI Lyα at $E = 6.97$ keV, respectively). We also note the presence of absorption residuals blueward of the main Fe K lines, likely associated with blueshifted highly ionized Fe resonance lines and edges. The Fe K emission and absorption are reminiscent of a P-Cygni line profile from a wind, as recently reported by Nardini et al. (2015) for the combined *XMM-Newton* and *NuSTAR* spectrum of the quasar PDS 456.

3.2. Accretion Disk Wind

The main objective of this analysis is to check if the *NuSTAR* data independently confirm the wind model found to provide the best fit for the *Suzaku* observation of IRAS F11119+3257 performed in 2013 (Tombesi et al. 2015).

In order to model the Fe K absorption, we then included a dedicated photoionization table using the *XSTAR* code version 2.2.1bn (Kallman & Bautista 2001). We consider a $\Gamma = 2$ power-law continuum, consistent with the observed value, and standard solar abundances (Asplund et al. 2009). We tested different broadenings due to turbulent velocities of 5000 km s^{-1}, 10,000 km s^{-1}, and 30,000 km s^{-1}. The latter provides the best fit and it is consistent with the large width observed for the absorption feature. This table is equivalent to the one used by Tombesi et al. (2015) to model the *Suzaku* spectrum.

This high turbulence value is introduced only to model the width of the absorption line and it is probably not linked to an actual physical turbulence in the gas. For instance, detailed accretion disk wind models show that the line profile becomes much broader because of the velocity shear between consecutive zones of the wind (e.g., Fukumura et al. 2010, 2014, 2015, 2017).

The output parameters of the *XSTAR* fit are the column density, ionization parameter, and the observed absorber redshift z_o. The ionization parameter is defined as $\xi = L_{ion}/(nr^2)$ erg s^{-1} cm (Tarter et al. 1969), where n is the number density of the material, and r is the distance of the gas from the central source. The observed absorber redshift is related to the intrinsic absorber redshift in the source rest frame z_a as $(1 + z_o) = (1 + z_a)(1 + z_c)$, where z_c is the cosmological redshift of the source. The velocity can then be determined using the relativistic Doppler formula $1 + z_a = (1 - \beta/1 + \beta)^{1/2}$, where $\beta = v/c$.

We obtain a high fit improvement of $\chi^2/\nu = 189/180$ ($\Delta\chi^2/\Delta\nu = 21/3$), indicating a requirement of the *XSTAR* absorber at the 99.97% according to the F-test ($\simeq 4\sigma$). The best-fit parameters are a column density of $N_H = (2.0^{+0.5}_{-0.3}) \times 10^{24}$ cm^{-2}, an ionization parameter of $\log \xi = 5.3^{+0.7}_{-0.5}$ erg s^{-1} cm, and an observed absorber redshift of $z_o = -0.18 \pm 0.03$. The power-law continuum slope is $\Gamma = 2.15 \pm 0.04$.

We then calculated an *XSTAR* emission table with the same parameters as for the absorption table and include it in the model to characterize the possible emission from the wind. The parameters of the emission table are column density, ionization, redshift, and normalization. We approximate the P-Cygni profile linking the ionization parameter and column density between the emission and absorption tables. We fix the redshift of the emitter to the cosmological redshift of the source and in order to parameterize the broadening of the emission feature we convolve the emission table with a Gaussian broadening profile.

The inclusion of the emission table provides an additional fit improvement of $\chi^2/\nu = 171/178$ ($\Delta\chi^2/\Delta\nu = 18/2$), which corresponds to a high statistical requirement of 99.98% according to the F-test ($\simeq 4\sigma$). The slope of the power-law continuum is now well constrained to be $\Gamma = 2.0 \pm 0.1$. The best-fit column density and ionization parameters are $N_H = (3.2 \pm 1.5) \times 10^{24}$ cm^{-2} and $\log \xi = 4.0^{+1.2}_{-0.3}$ erg s^{-1} cm, respectively.

The observed redshift of the absorber is estimated to be $z_o = -0.083^{+0.122}_{-0.058}$, which corresponds to an outflow velocity of $v_{out} = 0.253^{+0.061}_{-0.118}c$. The width of the emission line is $\sigma_E = 1.5^{+0.6}_{-0.4}$ keV, which corresponds to a velocity width of $\sigma_v = 0.21^{+0.09}_{-0.05}c$.

The *NuSTAR* spectrum and the best-fit wind model including both emission and absorption is shown in Figure 3. The combined statistical requirement of both emission and absorption components from the wind is very high, at the level of 5σ. We note that the best-fit parameters derived with *NuSTAR* are fully consistent with those estimated from the *Suzaku* spectrum and reported in Tombesi et al. (2015).

We note that the slope of the X-ray power-law continuum estimated to be $\Gamma = 2.0 \pm 0.1$ is consistent with the typical value for Seyferts and quasars (e.g., Dadina 2008). IRAS F11119+3257 is potentially accreting close to its Eddington value (Tombesi et al. 2015). Other very luminous quasars accreting at or beyond their Eddington value have been recently observed to host powerful UFOs and potentially
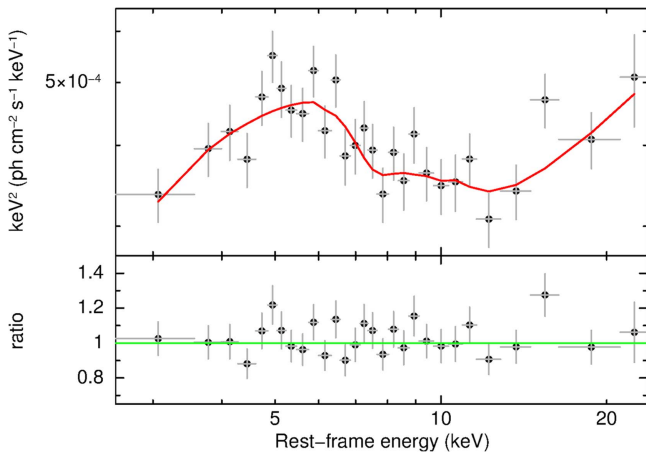
Figure 3. Upper panel: combined *NuSTAR* spectrum overlaid with the best-fit ionized emission and absorption wind model. Lower panel: ratio between the data and the best-fit model. The data are binned to a minimum signal-to-noise of 10 for clarity.

slightly steeper power-law slopes of $\Gamma \simeq 2.3$ when caught in high flux states (e.g., Lanzuisi et al. 2016; Matzeu et al. 2017).

The normalization of the emission table is $N = (7.2^{+2.5}_{-5.3}) \times 10^{-5}$. The normalization of the photo-ionized emission component is defined within the *XSTAR* code as $N = f L_{ion}/D^2$, where $f = \Omega/4\pi$ is the covering fraction of the material, L_{ion} is the ionizing luminosity in units of 10^{38} erg s^{-1} from 1 to 1000 Ryd (1 Ryd is 13.6 eV) and D is the distance of the observer to the source in kiloparsecs. This assumes a uniform, spherically symmetric, Compton-thin shell of material, which may be somewhat of an over-simplification for the emission from a disk wind. However, given the limited energy resolution of *NuSTAR* it should still provide a reasonable approximation of the emission line profile in a P-Cygni configuration.

If left free, the column density of the emitter and the normalization are degenerate. Assuming a column density linked to that of the absorber, as in the present case, we obtain an upper limit on the covering fraction f. Instead, assuming a covering fraction of unity, we would estimate a lower limit in the column density.

Substituting the appropriate values of the angular diameter distance $D \simeq 6.3 \times 10^5$ kpc and the extrapolated power-law ionizing luminosity of $L_{ion} \simeq 7 \times 10^6$ ($\times 10^{38}$) erg s^{-1}, we obtain a normalization of $N \simeq 2 \times 10^{-5}$ for $f = 1$. Comparing this value with the previous estimate, we derive the covering fraction of the wind is consistent with unity within the uncertainties. Alternatively, fixing the normalization to the value derived for $f = 1$ and performing a new fit, we estimate a lower limit on the column density of the emitter of $N_H \geqslant 1.3 \times 10^{24}$ cm^{-2}. Both fits provide the same χ^2/ν statistic. These tests support the fact that the emitter has both a high covering fraction ($f \simeq 1$) and a high column density ($N_H \geqslant 10^{24}$ cm^{-2}).

Although the wind parameters are well approximated with *XSTAR* absorption and emission tables, we note that a more physical model of a high column density wind should include both Compton scattering and line emission/reflection. Compton scattering may introduce a continuum break at an energy beyond the observed *NuSTAR* bandpass at $E > 50$ keV and it may contribute to the broadening of the lines of less than $\Delta E \simeq 0.3$ keV. A few detailed models have been reported in

the literature, but they are not publicly available for use in XSPEC and they require a relative fine-tuning of the parameters (e.g., Sim et al. 2010; Hagino et al. 2015). Even though our main conclusion will likely not change, as shown for instance for the wind in the quasar PDS 456 (e.g., Hagino et al. 2015; Nardini et al. 2015), we plan to employ more sophisticated wind models in future works.

3.3. Ionized Disk Reflection

We note that the curvature in the X-ray spectrum might be alternatively modeled as due to strong gravitational reflection from the inner accretion disk. Even though this possibility was already disfavored from the time-resolved spectral analysis of the *Suzaku* data reported in Tombesi et al. (2015), here we consider again this possibility using the average *NuSTAR* spectrum.

We use the most accurate relativistic reflection code available in the literature, the *relxilllp* model (García et al. 2014). This model considers a lamp-post geometry in which the compact X-ray emitting source is located on the rotation axis of the black hole at a certain height in units of gravitational radii $r_g = GM_{BH}/c^2$. The reflection fraction and emissivity index are estimated depending on the source height and black hole spin. In order to allow for the largest possible relativistic broadening, we consider the case of a maximally spinning black hole. We also assume a typical outer disk radius of $r_{out} = 400 r_g$, and the inner radius r_{in} is linked to the innermost stable circular orbit. We consider standard solar abundances, but we checked also the case of free Fe abundance. The high-energy cutoff is assumed at the typical value of $E_c \simeq 100$ keV (Malizia et al. 2014; Fabian et al. 2015; Ricci et al. 2017). Then, the free parameters of the model are the height of the illuminating source h, the disk inclination angle i, the ionization parameter $\log \xi$, and the normalization.

Initially, we checked if the relativistically broadened disk reflection model alone could describe the *NuSTAR* spectrum, considering a solar abundance for iron. From a statistical point of view, we obtain a good fit ($\chi^2/\nu = 176/180$) with an inclination of $i = 59^{+6}_{-8}$ degrees, ionization parameter $\log \xi = 3.3 \pm 0.2$ erg s^{-1} cm, and power-law slope $\Gamma = 2.0 \pm 0.1$. However, the fit is rather extreme considering the other physical parameters. In fact, the height of the compact emitting source is pegged to the hard lower limit of $h = 3 r_g$, with a 90% upper limit of $h < 35 r_g$. Moreover, the reflection fraction would be rather high, $R \simeq 4$, requiring a reflection dominated spectrum. Leaving the Fe abundance free to vary it provides only a marginal improvement to the fit ($\Delta\chi^2/\Delta\nu = 3/1$), with the value pegged to the hard upper limit of 10. Recent papers questioned the physical reliability of such extreme parameters (e.g., Dovčiak & Done 2016).

We then checked the possibility to have both relativistic disk reflection and wind absorption combining both the *relxilllp* emission and *XSTAR* absorption tables. This is phenomenologically similar to what we may expect to see from a Compton-thick wind, which is launched close to the black hole. Indeed, we obtain a fit ($\chi^2/\nu = 171/177$) with a disk inclination of $i = 60^{+27}_{-10}$ deg, ionization parameter $\log \xi = 3.5^{+0.6}_{-0.4}$ erg s^{-1} cm, and power-law slope $\Gamma = 2.0^{+0.5}_{-0.1}$. The source height is again pegged to the lower limit of $h = 3 r_g$, and we derive a 90% upper limit of $h < 28 r_g$. The absorber is found to have a column density of $N_H = (1.7^{+2.2}_{-0.9}) \times 10^{23}$ cm^{-2}, ionization

Table 1
Average Parameters of The Ultra-fast Outflow in IRAS F11119+3257
Observed with *Suzaku* and *NuSTAR*

Satellite	Year	$\log \xi$ (erg s^{-1} cm)	N_H (10^{24} cm^{-2})	v_{out} (c)	P (σ)
Suzaku	2013	$4.11^{+0.09}_{-0.04}$	$6.4^{+0.8}_{-1.3}$	0.255 ± 0.011	6.5
NuSTAR	2015	$4.0^{+1.2}_{-0.3}$	3.2 ± 1.5	$0.253^{+0.061}_{-0.118}$	5.0

Note. Columns: satellite name; observation year; ionization parameter; column density; outflow velocity; detection significance.

parameter of $\log \xi = 2.5^{+0.9}_{-0.5}$ erg s^{-1} cm, and a less constrained velocity shift of $v_{out} = 0.13^{+0.13}_{-0.11}c$.

From a purely statistical point of view, the relativistic disk reflection plus wind absorption model is equivalent to the P-Cygni wind emission/absorption model discussed in the previous section. This is similar to what we reported in Tombesi et al. (2015) for the time-averaged *Suzaku* spectrum of IRAS F11119+3257. However, in Tombesi et al. (2015), we demonstrated that the wind model was preferred to the relativistic disk reflection model because it provided a simple explanation of the source flux variability as due to a change in absorber column density. In contrast, within the relativistic reflection model, the resultant variability pattern would be the opposite of that expected from the relativistic light bending model (Miniutti & Fabian 2004). Furthermore, the extrapolated hard X-ray luminosity in the energy band $E = 14$–195 keV from the fast wind model matches the value expected from mid-infrared emission line diagnostics, while the relativistic reflection model underestimated this value by more than one order of magnitude (Tombesi et al. 2015).

4. Discussion

4.1. The UFO

In the previous sections, we reported the analysis of the *NuSTAR* spectrum of IRAS F11119+3257. The main objective of this project is to perform an independent check of the results derived from the *Suzaku* observation reported in Tombesi et al. (2015). Indeed, we clearly detect a highly ionized Fe K wind in the *NuSTAR* spectrum. The best-fit parameters are a column density of $N_H = (3.2 \pm 1.5) \times 10^{24}$ cm^{-2}, an ionization parameter of $\log \xi = 4.0^{+1.2}_{-0.3}$ erg s^{-1} cm, and an outflow velocity of $v_{out} = 0.253^{+0.061}_{-0.118}c$.

These wind parameters are consistent with the ones reported in Tombesi et al. (2015) for the average *Suzaku* spectrum obtained in 2013, see Table 1. The ionization and velocity of the wind seems to be stable on a timescale of at least two years, spanning between the *Suzaku* and *NuSTAR* observations. Instead, already from the long *Suzaku* observation, the absorber column density was found to vary between $N_H \simeq (3$–$9) \times 10^{24}$ cm^{-2} on a timescale as short as three days. This may suggest clumpiness in the wind, as already reported for other quasar disk winds (e.g., Matzeu et al. 2016; Reeves et al. 2016).

Given the best-fit parameters of the wind estimated from *NuSTAR*, we can estimate the energetics of the wind following the approach described in Tombesi et al. (2015). The mass of the central supermassive black hole in IRAS F11119+3257 is estimated to be $\log M_{BH} = 7.2 \pm 0.5\, M_\odot$ (Kawakatu et al. 2007). A lower limit on the location of the absorber

can be derived from the radius at which the observed velocity corresponds to the escape velocity, $r = 2GM_{BH}/v_{out}^2 \simeq 7.4 \times 10^{13}$ cm. Converting in units of Schwarzschild radii, the wind launching radius is likely at a distance of $r \geqslant 16\, r_s$ from the central black hole.

The mass outflow rate of the wind can be estimated considering the equation $\dot{M}_{out} = 4\pi\mu m_p r N_H C_F v_{out}$, where $\mu = 1.4$ is the mean atomic mass per proton, m_p is the proton mass, and C_F is the wind covering fraction (Crenshaw & Kraemer 2012). In spherical symmetry, this latter value corresponds to the solid angle subtended by the wind of $\Omega = 4\pi C_F$. A high covering fraction $C_F \simeq 1$ was estimated in IRAS F11119+3257 by Tombesi et al. (2015) and in the quasar PDS 456 (Nardini et al. 2015). Conservatively, here we assume $C_F \simeq 0.5$ estimated from the fraction of sources with detected UFOs and warm absorbers (e.g., Tombesi et al. 2010, 2013, 2014; Crenshaw & Kraemer 2012; Gofford et al. 2013). Therefore, we conservatively estimate a lower limit on the mass outflow rate of $\dot{M}_{out} \simeq 0.5\, M_\odot$ yr^{-1}.

Given the high luminosity of this AGN and the SMBH mass estimate, this source may likely be accreting at a rate close or slightly higher than Eddington. Mildly super-Eddington sources are likely to host powerful disk winds and it is likely that the AGN radiation contributes significantly to driving the wind (e.g., Matzeu et al. 2017). For a highly ionized wind driven mostly by radiation pressure due to Compton scattering, we have the relation $\dot{P}_{out} = \tau C_F \dot{P}_{AGN}$ (e.g., Reynolds 2012; Tombesi et al. 2013, 2015; Matzeu et al. 2017), where $\dot{P}_{out}$ and $\dot{P}_{AGN}$ are the momentum rates of the wind and AGN radiation, respectively. Considering a covering fraction $C_F \simeq 1$ and the optical depth of $\tau \simeq 2$ derived from the wind column density, we can estimate $\dot{P}_{out} \simeq 2\dot{P}_{AGN}$ to be the upper limit for a radiation driven wind. Substituting $\dot{P}_{AGN} = L_{AGN}/c$, $\dot{P}_{out} = \dot{M}_{out} v_{out}$, and $L_{AGN} \simeq 1.5 \times 10^{46}$ erg s^{-1} (Veilleux et al. 2013), we can estimate an upper limit on the mass outflow rate of $\dot{M}_{out} \simeq 2\, M_\odot$ yr^{-1}. Therefore, the wind mass outflow rate is likely in the range of $\dot{M}_{out} \simeq 0.5$–$2\, M_\odot$ yr^{-1}. The momentum flux (or force) and mechanical (or kinetic) power of the wind are then estimated to be $\dot{P}_{out} \simeq (2.5$–$10) \times 10^{35}$ dyne and $\dot{E}_{out} = (1/2)\dot{M}_{out} v_{out}^2 \simeq (1-4) \times 10^{45}$ erg s^{-1}, respectively.

Comparing the wind energetics with the AGN luminosity, we obtain $\dot{P}_{out} \simeq 0.5$–$2\, \dot{P}_{AGN}$ and $\dot{E}_{out} \simeq 7\%$–$27\%\, L_{AGN}$, respectively. We note that the wind parameters estimated from *NuSTAR* are consistent with the ones derived from *Suzaku* in Tombesi et al. (2015). In fact, in the *Suzaku* case, we obtained $\dot{M}_{out} \simeq 1.5$–$4.5\, M_\odot$ yr^{-1}, $\dot{P}_{out} \simeq 0.4$–$3\, \dot{P}_{AGN}$, and $\dot{E}_{out} \simeq 5\%$–$42\%\, L_{AGN}$, respectively. The UFO is consistent with having a momentum rate equivalent to that of the AGN radiation and the energetics is high enough to have an influence in AGN feedback (e.g., Di Matteo et al. 2005; Hopkins & Elvis 2010; Gaspari et al. 2011).

4.2. Connection with Galaxy-scale Molecular Outflows

Comparing the energetics of the X-ray UFO detected with *Suzaku* and the OH molecular outflow detected with *Herschel* in IRAS F11119+3257, we found that the favored interpretation of the connection between the two winds was provided by the energy-conserving relation $\dot{P}_{out} \simeq f(v_X/v_G)(L_{AGN}/c)$, where v_X is the velocity of the inner X-ray wind, v_G is the velocity of the galaxy-scale molecular outflow, and f is the ratio between the covering fractions of the outer molecular outflow and inner disk wind (Tombesi et al. 2015). Instead, in the case

of momentum-conserving, we would expect a relation $\dot{P}_{out} \simeq L_{AGN}/c$.

Here, we consider the wind parameters derived from *NuSTAR* and compare them with the latest estimates of the OH and CO molecular outflows in IRAS F11119+3257 reported by Veilleux et al. (2017). The OH molecular outflow detected with *Herschel* is estimated to have a maximum velocity of $v_{out} \simeq 1000 \, \mathrm{km \, s^{-1}}$, a mass outflow rate of $\dot{M}_{out} \simeq 250–2000 \, M_{\odot} \, \mathrm{yr^{-1}}$, a momentum rate of $\dot{P}_{out} \simeq 3.5–25 \, L_{AGN}/c$, a mechanical energy $\dot{E}_{out} \simeq 0.5\%–5\% \, L_{AGN}$, and a distance of $d \simeq 0.1–1$ kpc from the central black hole. The parameters of the CO molecular outflow detected with *ALMA* are a maximum velocity of $v_{out} \simeq 1000 \, \mathrm{km \, s^{-1}}$, a mass outflow rate of $\dot{M}_{out} \simeq 400–1000 \, M_{\odot} \, \mathrm{yr^{-1}}$, a momentum rate of $\dot{P}_{out} \simeq 8–16 \, L_{AGN}/c$, a mechanical energy of $\dot{E}_{out} \simeq 0.8\%–2\% \, L_{AGN}$, and a distance of $d \sim 4–15$ kpc.

We note that in both cases the outflow momentum rate is about a factor of 10 higher than that in the radiation field and the energetics is up to a few percent of the AGN luminosity. Considering the energy-conserving relation previously described and substituting the relative parameters, we find that the inner UFO would indeed be able to drive the observed molecular outflows with momentum rates of $\dot{P}_{out} \simeq 15 \, L_{AGN}/c$.

However, we should bear in mind that the estimates of the mass outflow rates may be affected by systematics and the conclusion may be less stringent. In fact, the most conservative estimates derived by Veilleux et al. (2017) indicate that the OH and CO molecular outflows may have momentum rates in the range $\dot{P}_{out} \simeq 1–6 \, L_{AGN}/c$ and $\dot{P}_{out} \simeq 1.5–3 \, L_{AGN}/c$, respectively. Therefore, even if unlikely, the momentum-conserving regime cannot be fully excluded in this case. Moreover, we should consider the caveat that the fast X-ray wind is observed now, while the large-scale molecular outflows are probably an integrated effect of such winds over a much longer period of time. Deep and spatially resolved soft X-ray and radio observations may help to distinguish between energy- or momentum-conserving flows given that the emission from the shocked gas is expected to be different in these two cases (e.g., Bourne & Nayakshin 2013; Nims et al. 2015). Some attempts have been reported in the literature (e.g., Zakamska & Greene 2014; Tombesi et al. 2017).

5. Conclusions

In Tombesi et al. (2015), we reported the detection of a powerful UFO in the *Suzaku* X-ray spectrum of the ultra-luminous infrared galaxy IRAS F11119+3257. The comparison with a galaxy-scale OH molecular outflow observed with *Herschel* in the same source supported the energy-conserving scenario for AGN feedback. In this work, we perform an independent check of the *Suzaku* results using the higher sensitivity and wider X-ray continuum coverage of *NuSTAR*.

We clearly detect a highly ionized Fe K UFO in the 100 ks *NuSTAR* spectrum with parameters $N_H = (3.2 \pm 1.5) \times 10^{24} \, \mathrm{cm^{-2}}$, $\log \xi = 4.0^{+1.2}_{-0.3} \, \mathrm{erg \, s^{-1} \, cm}$, and $v_{out} = 0.253^{+0.061}_{-0.118} \, c$. The wind launching radius is likely at a distance of $r \geqslant 16 r_s$ from the central black hole. The mass outflow rate is in the range of $\dot{M}_{out} \simeq 0.5–2 \, M_{\odot} \, \mathrm{yr^{-1}}$. The UFO momentum rate and power are $\dot{P}_{out} \simeq 0.5–2 L_{AGN}/c$ and $\dot{E}_{out} \simeq 7\%–27\% \, L_{AGN}$, respectively. The UFO parameters are consistent between the 2013 *Suzaku* and the 2015 *NuSTAR* observations. Only the column density is found to be variable, possibly suggesting clumps in the wind.

New multi-wavelength campaigns involving X-ray and optical, infrared, millimeter, and radio observatories of this source and a larger population of luminous quasars will allow us to constrain the physical details of the AGN feedback processes and to determine if it is indeed widespread as expected from numerical simulations of galaxy evolution (e.g., Fiore et al. 2017). In the X-ray domain, transformative new results are expected from the unprecedented spectroscopic capabilities of the planned X-ray astronomy recovery mission (*XARM*; Hitomi Collaboration et al. 2016) and the *Athena* X-ray observatory (Cappi et al. 2013; Nandra et al. 2013).

ORCID iDs

F. Tombesi https://orcid.org/0000-0002-6562-8654
S. Veilleux https://orcid.org/0000-0002-3158-6820
M. Meléndez https://orcid.org/0000-0001-8485-0325

References

Asplund, M., Grevesse, N., Sauval, A. J., & Scott, P. 2009, ARA&A, 47, 481
Bourne, M. A., & Nayakshin, S. 2013, MNRAS, 436, 2346
Cappi, M., Done, C., Behar, E., et al. 2013, arXiv:1306.2330
Cicone, C., Maiolino, R., Sturm, E., et al. 2014, A&A, 562, A21
Costa, T., Sijacki, D., & Haehnelt, M. G. 2014, MNRAS, 444, 2355
Crenshaw, D. M., & Kraemer, S. B. 2012, ApJ, 753, 75
Dadina, M. 2008, A&A, 485, 417
Di Matteo, T., Springel, V., & Hernquist, L. 2005, Natur, 433, 604
Dovčiak, M., & Done, C. 2016, AN, 337, 441
Fabian, A. C., Lohfink, A., Kara, E., et al. 2015, MNRAS, 451, 4375
Faucher-Giguère, C.-A., & Quataert, E. 2012, MNRAS, 425, 605
Feruglio, C., Fiore, F., Carniani, S., et al. 2015, A&A, 583, A99
Fiore, F., Feruglio, C., Shankar, F., et al. 2017, A&A, 601, A143
Fukumura, K., Kazanas, D., Contopoulos, I., & Behar, E. 2010, ApJ, 715, 636
Fukumura, K., Kazanas, D., Shrader, C., et al. 2017, NatAs, 1, 0062
Fukumura, K., Tombesi, F., Kazanas, D., et al. 2014, ApJ, 780, 120
Fukumura, K., Tombesi, F., Kazanas, D., et al. 2015, ApJ, 805, 17
García, J., Dauser, T., Lohfink, A., et al. 2014, ApJ, 782, 76
Gaspari, M., Brighenti, F., D'Ercole, A., & Melioli, C. 2011, MNRAS, 415, 1549
Gaspari, M., & Sądowski, A. 2017, ApJ, 837, 149
Gofford, J., Reeves, J. N., McLaughlin, D. E., et al. 2015, MNRAS, 451, 4169
Gofford, J., Reeves, J. N., Tombesi, F., et al. 2013, MNRAS, 430, 60
González-Alfonso, E., Fischer, J., Graciá-Carpio, J., et al. 2014, A&A, 561, A27
González-Alfonso, E., Fischer, J., Spoon, H. W. W., et al. 2017, ApJ, 836, 11
Hagino, K., Odaka, H., Done, C., et al. 2015, MNRAS, 446, 663
Hitomi Collaboration, Aharonian, F., Akamatsu, H., et al. 2016, Natur, 535, 117
Hopkins, P. F., & Elvis, M. 2010, MNRAS, 401, 7
Hopkins, P. F., Hernquist, L., Cox, T. J., et al. 2006, ApJS, 163, 1
Kalberla, P. M. W., Burton, W. B., Hartmann, D., et al. 2005, A&A, 440, 775
Kallman, T., & Bautista, M. 2001, ApJS, 133, 221
Kawakatu, N., Imanishi, M., & Nagao, T. 2007, ApJ, 661, 660
King, A. 2003, ApJL, 596, L27
King, A. R., & Pounds, K. A. 2003, MNRAS, 345, 657
Lanzuisi, G., Perna, M., Comastri, A., et al. 2016, A&A, 590, A77
Longinotti, A. L., Krongold, Y., Guainazzi, M., et al. 2015, ApJL, 813, L39
Malizia, A., Molina, M., Bassani, L., et al. 2014, ApJL, 782, L25
Matzeu, G. A., Reeves, J. N., Nardini, E., et al. 2016, MNRAS, 458, 1311
Matzeu, G. A., Reeves, J. N., Nardini, E., et al. 2017, MNRAS, 465, 2804
Miniutti, G., & Fabian, A. C. 2004, MNRAS, 349, 1435
Nandra, K., Barret, D., Barcons, X., et al. 2013, arXiv:1306.2307
Nardini, E., Reeves, J. N., Gofford, J., et al. 2015, Sci, 347, 860
Nims, J., Quataert, E., & Faucher-Giguère, C.-A. 2015, MNRAS, 447, 3612

Parker, M. L., Pinto, C., Fabian, A. C., et al. 2017, Natur, 543, 83
Reeves, J. N., Braito, V., Nardini, E., et al. 2016, ApJ, 824, 20
Reynolds, C. S. 2012, ApJL, 759, L15
Ricci, C., Trakhtenbrot, B., Koss, M. J., et al. 2017, arXiv:1709.03989
Silk, J., & Rees, M. J. 1998, A&A, 331, L1
Sim, S. A., Miller, L., Long, K. S., Turner, T. J., & Reeves, J. N. 2010, MNRAS, 404, 1369
Sturm, E., González-Alfonso, E., Veilleux, S., et al. 2011, ApJL, 733, L16
Tarter, C. B., Tucker, W. H., & Salpeter, E. E. 1969, ApJ, 156, 943
Teng, S. H., & Veilleux, S. 2010, ApJ, 725, 1848
Tombesi, F., Cappi, M., Reeves, J. N., et al. 2010, A&A, 521, A57

Tombesi, F., Cappi, M., Reeves, J. N., et al. 2011, ApJ, 742, 44
Tombesi, F., Cappi, M., Reeves, J. N., et al. 2013, MNRAS, 430, 1102
Tombesi, F., Cappi, M., Reeves, J. N., & Braito, V. 2012, MNRAS, 422, L1
Tombesi, F., Meléndez, M., Veilleux, S., et al. 2015, Natur, 519, 436
Tombesi, F., Mushotzky, R. F., Reynolds, C. S., et al. 2017, ApJ, 838, 16
Tombesi, F., Tazaki, F., Mushotzky, R. F., et al. 2014, MNRAS, 443, 2154
Veilleux, S., Bolatto, A., Tombesi, F., et al. 2017, ApJ, 843, 18
Veilleux, S., Meléndez, M., Sturm, E., et al. 2013, ApJ, 776, 27
Wagner, A. Y., Umemura, M., & Bicknell, G. V. 2013, ApJL, 763, L18
Zakamska, N. L., & Greene, J. E. 2014, MNRAS, 442, 784
Zubovas, K., & King, A. 2012, ApJL, 745, L34